

Synoptic climatology associated with heavy rainfall events in the Itajaí Valley region, Brazil

Gustavo Carlos Juan ESCOBAR^{1*} and Marcelo BARBIO ROSA²

¹ Instituto Nacional de Pesquisas Espaciais (INPE), 12630-000, Cachoeira Paulista, SP, Brazil.

² Instituto Nacional de Pesquisas Espaciais (INPE), 12227-900, São José dos Campos, São Paulo, Brazil.

*Corresponding author: gustavo.escobar@inpe.br

Received: December 14, 2023; Accepted: April 30, 2024

RESUMEN

Este estudio presenta una climatología sinóptica de eventos de lluvia fuerte (ELLF) en la región del Valle de Itajaí (rVI) en la parte este del estado de Santa Catarina (SC) entre 2000 y 2022. Se identificaron un total de 195 ELLF, correspondientes a precipitaciones superiores a 27 mm diarios. El patrón sinóptico medio asociado con los ELLF mostró el avance de un frente frío sobre la región de estudio y la presencia de un sistema de baja presión sobre el noreste de Argentina y Paraguay, el cual provocó advección cálida sobre gran parte del estado de SC. Este patrón también se observó en el nivel de 850 hPa, donde las circulaciones ciclónicas centradas sobre Paraguay dos días antes (día -2) de los ELLF intensificaron el transporte de humedad desde la región amazónica sobre SC. El día 0 se observó una vaguada en la troposfera media y superior sobre Argentina, Uruguay y partes del sur de Brasil, mostrando un sistema dinámico típico de latitudes medias que refleja el frente frío observado en superficie. La clasificación sinóptica en superficie identificó cuatro patrones sinópticos principales asociados con ELLF en la rVI. El patrón más frecuente estuvo relacionado con la presencia del Anticiclón Subtropical del Atlántico Sur (ASAS) con características de bloqueo. Dos patrones estuvieron relacionados con un típico frente frío, y el último patrón estuvo asociado con un proceso ciclogénico. No se encontró correlación entre la temperatura superficial del mar (TSM) y la ocurrencia de ELLF en la rVI; sin embargo, el gradiente de anomalía de TSM observado alrededor de la latitud 35° S sugiere que los frentes fríos pueden estar anclados sobre una zona de aguas anormalmente frías en la costa sur de Brasil.

ABSTRACT

This study presents a synoptic climatology of heavy rainfall events (HRE) in the Itajaí Valley region (IVr) in the eastern Santa Catarina (SC) state between 2000 and 2022. A total of 195 HRE were identified, corresponding to accumulations greater than 27 mm per day. The mean synoptic pattern associated with HRE showed the presence of a cold front over the study region and a low-pressure system over northeastern Argentina and Paraguay that promoted warm advection over much of the SC state. This pattern was also observed at the 850 hPa level, where a cyclonic circulation centered over Paraguay two days before the HRE (day -2) intensified the moisture transport from the Amazon region over SC. On day 0, a trough in the middle and upper troposphere was observed over Argentina, Uruguay, and parts of southern Brazil, showing a typical mid-latitude dynamic system that reflects the cold front observed at the surface. The synoptic classification identified four main surface synoptic patterns associated with HRE in the IVr. The most frequent pattern was related to the presence of the South Atlantic Subtropical Anticyclone (SASA) with blocking characteristics. Two patterns were related to a typical cold front, and the last was associated with a cyclogenetic process. No correlation was found between the sea surface temperature (SST) and the occurrence of HRE in the IVr; however, the SST anomaly gradient observed around 35° S suggested that cold fronts may be anchoring over the region of anomalously cold waters over the coast of the south of Brazil.

Keywords: synoptic climatology, Itajaí Valley region, cold front, blocking type anticyclone.

1. Introduction

The Itajaí Valley region (IVr) is in the eastern part of Santa Catarina (SC) state. It is the most vulnerable area of the state due to its high susceptibility to flooding and landslides during heavy rainfall events (HRE) (Herrmann, 2014; Ávila and Mattedi, 2017; Cardoso, 2017; Murara et al., 2018). The IVr has a complex topography characterized by mountains and valleys that modify the atmospheric flow and influence the local weather patterns by, for instance, enhancing the rainfall intensity and, therefore, producing localized HRE.

Cold fronts are the most common synoptic-scale meteorological systems that modify weather conditions in the central-southern region of the South American continent (Andrade, 2005; Escobar et al., 2019a). According to Foss et al. (2017), there are two preferred regions with a higher frequency of cold front passages over South America: the first is located immediately east of the Andes Mountains, and the second is along the coast of the south and southeast regions of Brazil. Thus, the IVr is one of the regions with the highest frequency of cold front passages in Brazil.

Escobar et al. (2016) performed a synoptic climatology of cold fronts associated with HRE in the IVr, based on 32 years (1979-2010) of data from the Climate Forecast System Reanalysis (CFSR) of the National Center for Environmental Prediction (NCEP). The authors found that the most frequent synoptic pattern shows an intense surface southeasterly wind over the studied area, determined by a strong post-frontal anticyclone located over southern Buenos Aires state in Argentina. In this case, the associated cold front is in the extreme northeastern part of the SC state.

The Upper-Level Cyclonic Vortex (ULCV) is another synoptic-scale meteorological system that influences the weather over the IVr throughout the year and produces severe weather events with strong impacts on the population. From November 21 to 24, 2008, this upper-level low-pressure system was responsible for one of the biggest natural disasters in the state of SC (Silva Dias, 2009; García et al., 2011). The eastern SC was affected by an atmospheric blocking configuration, determined by the presence of an intense anticyclone in the South Atlantic Ocean (SAO) and the action of a ULCV at

500 hPa located within the state of SC. Both systems determined an atmospheric circulation at the surface that favored the intensification of northeasterly winds over eastern SC, contributing to heavy rainfall in the IVr. Between November 22 and 23, rainfall records showed accumulations of up to 300 mm in the IVr. The cities of Blumenau, Florianópolis, Indaial, and Joinville were also affected and presented strong impacts on the population. In summary, 60 cities and 1.5 million people were affected, 9390 were displaced, and 135 died.

Extratropical and subtropical cyclones (Taljaard, 1972; Simmonds and Keay, 2000; Hoskins and Hodges, 2005) are other of the main synoptic-scale weather systems that cause HRE in the eastern part of the SC state, including the IVr. Most of these cyclones are extratropical, but they can also exhibit subtropical (Gozzo et al., 2014; Reboita et al., 2022) or tropical characteristics (McTaggart-Cowan et al., 2006) on many occasions. The formation process and cyclonic circulation associated with these weather systems contribute to the intensification of winds and rainfall in the IVr. Among the various extratropical cyclones, it can be mentioned the explosive cyclone (Sanders and Gyakum, 1980; Seluchi and Saulo, 1998; Lim and Simmonds, 2002) occurred between June 30 and July 1, 2020, when a squall line crossed the SC state during the formation process, causing severe weather with strong impacts in various locations, including the IVr (Fortunato et al., 2023).

Considering that the HRE occurring in the IVr under the influence of synoptic-scale weather systems can significantly impact the local population, understanding the behavior of these episodes is crucial for urban planners to minimize their effects. Therefore, this study aims to develop a synoptic climatology to describe the dynamic and thermodynamic characteristics associated with these events, given the importance of these weather systems in modulating precipitation in this vulnerable region (Ávila and Mattedi, 2017; Murara et al., 2018). Furthermore, most studies associated with HRE in the IVr are either based on synoptic analyses of specific cases or statistical studies of mean meteorological conditions. Therefore, another objective of this study is to analyze the variability of atmospheric circulation associated with these extreme events by creating a surface synoptic classification. The main synoptic

patterns of HRE in the IVr obtained in this work may also help weather forecasters to improve their forecasting and minimize the impacts of flooding and landslides in vulnerable regions.

This paper is organized as follows: section 2 details the data and the methodology used in this study; section 3 analyzes the synoptic features and identifies the principal surface weather patterns associated with HRE in the IVr, and section 4 presents the conclusions.

2. Data and methodology

2.1 Data

To identify the HRE in the IVr, daily precipitation data from the period 2000-2022 were used, obtained through the MERGE product (Escobar et al., 2016, 2022), with a spatial resolution of $0.2^\circ \times 0.2^\circ$. MERGE results from combining surface observations over the South American continent with Tropical Rainfall Measuring Mission (TRMM) satellite precipitation estimates (Rozante et al., 2010).

Images captured by the Geostationary Operational Environmental Satellite (GOES) series, specifically in the thermal infrared (IR) channels (Knapp et al., 2011), were acquired with a spatial resolution of 0.1° at 12:00 UTC. These images were used to pinpoint the cloudiness linked with the HRE in the IVr region.

Weekly sea surface temperature (SST) data derived from NOAA Optimum Interpolation (OI) SST V2 High Resolution with a spatial resolution of 0.25° (Huang et al., 2021) was also used for the period 2000-2022.

To study the synoptic characteristics associated with HRE in the IVr, daily (12:00 UTC), gridded reanalysis meteorological data from the National Centers for Environmental Prediction (NCEP) Climate Forecast System Reanalysis (CFSR) were used for the period 2000-2022. The CFSR v. 1 (Saha et al., 2010) covers the period from January 1979 to March 2011, and the CFSR v. 2 (Saha et al., 2014) was released in March 2011 and has been running operationally since then. Both have a horizontal native resolution of T382 (~ 38 km). Their horizontal resolution is $0.25^\circ \times 0.25^\circ$ between 10° S and 10° N, reducing gradually towards the poles, reaching 0.5° between 30° N and 30° S. We selected the 12:00 UTC datasets due to the higher density of observations over

the South American continent at this time; therefore, the analysis is expected to be more accurate.

The CFSR meteorological variables used are: (i) mean sea level pressure (hPa); (ii) 850 hPa specific humidity (g kg^{-1}), and 850, 500 and 250 hPa wind components (m s^{-1}); (iii) 850, 500 and 250 hPa geopotential height (gpm), and (iv) 500 hPa temperature ($^\circ\text{C}$) for the period 2000-2022. We also utilized surface synoptic charts at 12:00 UTC from the Brazilian Center for Weather Forecast and Climate Studies (CPTEC), National Institute for Space Research (INPE), spanning from 2010 to 2022.

2.2 Selection of HRE

According to Teixeira and Satyamurty (2007), the definition of HRE is subjective and varies significantly from one study to another. HRE is usually based on a precipitation threshold, while in other cases, it is determined by comparing the precipitation averaged over a reasonably wide area. As the focus of this study is to identify the synoptic pattern associated with the onset of HRE rather than its persistence, only the first day of HRE is considered.

In this study, HRE were selected using the percentile technique (Dereczynski et al., 2009; Silva and Reboita, 2013; Escobar et al., 2016), which involves calculating daily precipitation quantiles based on the average precipitation in a selected area (red box in Fig. 1a) using MERGE rainfall data with a spatial resolution of $0.2^\circ \times 0.2^\circ$. The grid of the MERGE rainfall is depicted in Figure 1b. Thus, we obtained a unified value representing the daily precipitation in the box. In the specified region, rainfall values above the 95th percentile (the top 5% of the most intense cases from the total number of events) were considered, corresponding to accumulations greater than 27 mm day^{-1} . As a result, 195 cases of HRE were identified.

2.3 Composites fields

After the selection of the HRE, average composite fields of atmospheric variables mentioned in section 2.1 for two days before the initial day (day -2) and at the initial HRE day (day 0) were calculated to identify the synoptic features associated with such episodes. The maps comprise the domain of 5° - 40° S and 80° - 30° W for all variables. Mean fields are constructed for the whole period, from 2000 to 2022.

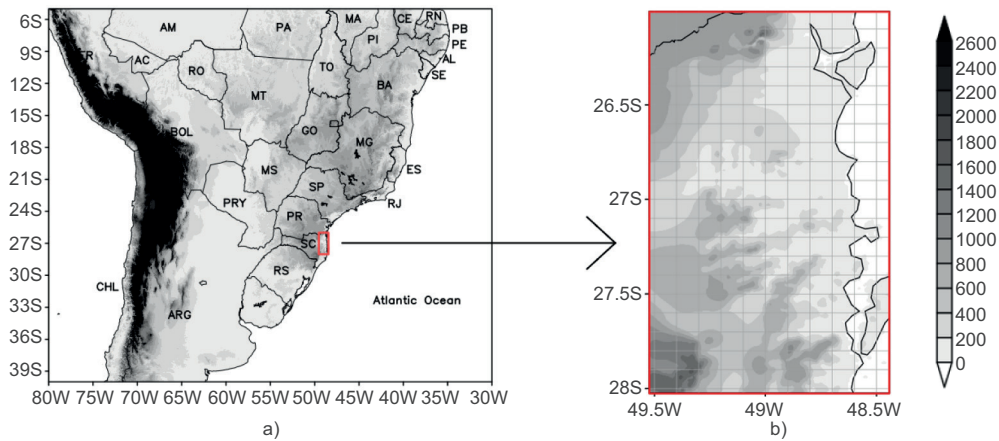


Fig. 1. (a) Area selected for study. The red box indicates the Itajaí Valley region; (b) grid of the merged rainfall data within the area selected. Shaded areas represent orography in meters.

The weekly SST anomaly is calculated from the weekly SST climatology, then all event anomalies are averaged to create the composite. The weekly SST climatology was obtained for the whole period, from 2000 to 2022.

2.4 Synoptic classification

After identifying the mean synoptic features associated with HRE in the IVr, a synoptic classification at the surface was performed through principal pattern sequence analysis (PPSA) (Compagnucci et al., 2001; Escobar et al., 2004; Huth et al., 2008). According to Compagnucci et al. (2001), PPSA is considered an extension of the traditional principal component analysis (PCA), with a correlation matrix in T-mode (Green and Carrol, 1978; Richman, 1986; Escobar et al., 2016). The main objective is to obtain the evolution of the principal dominant modes of atmospheric circulation for specific meteorological situations. In this application, each variable is a sequence of consecutive spatial mean sea level pressure patterns, and the correlation matrix represents the correlation between sequences.

The matrices are composed of mean sea level pressure data of the 195 HRE \times 7171 grid points for three days: two days before the initial day (day -2), one day before the initial day (day -1), and the initial HRE day (day 0). With such an objective methodology, it is possible to identify subgroups or types of fields with the same spatial structure.

After the application of the PPSA, varimax rotation (Richman, 1986) was performed. This

methodology is useful to redistribute the total variance of data among the components to emphasize the physical meaning of the principal pattern sequence (PPS) (Richman, 1986). The optimum number of rotated PPSs was determined by the eigenvalue 1.0 rule (Richman et al., 1992). The real meteorological fields significantly correlated with the PPSs were determined through a temporal series of factor loadings representing the correlations between the variable used (real meteorological field) and each PPS (Richman, 1986). Analysis of the component loadings allows the evaluation of representative patterns (obtained from PPSA) as real atmospheric circulation fields (registered in the reanalysis). Values of component loadings closer to 1 represent sequences of atmospheric circulation fields similar to the obtained pattern sequence (Harman, 1976; Cattell, 1978).

The spatial field of the PPSs can be interpreted in both positive and negative phases (Compagnucci and Salles, 1997). Moreover, PPSs are related to two different synoptic patterns with the same shape. For positive values of component loadings (direct mode), PPSs have the same sign as the meteorological variable under study. For example, positive (negative) values of sea level pressure represent high (low) pressures in the PPSs. Conversely, for negative values of component loadings (indirect mode), PPSs have the opposite sign as the real meteorological fields, that is, positive (negative) values represent low (high) pressures. In this study, the values of component loadings (figures not shown) were positive, meaning that

the PPSs have the same sign as the meteorological fields (weather type).

Finally, the seasonal variation of the variance explained by each PPS found at the surface was calculated to determine the respective contributions or weights of each PPS during different seasons of the year: summer (December, January, February), autumn (March, April, May), winter (June, July, August), and spring (September, October, November). These explained variances were computed using the respective series of component loadings (Harman 1976; Cattell 1978).

3. Results

3.1 Climatology of HRE in the IVr

Figure 2 shows the annual distribution of the number of HRE cases in the IVr. There are two similar main maxima; one in January and the other in September. The highest concentration of HRE in the IVr is observed in spring, mainly during September and October, with 26 and 23 cases, respectively. This characteristic is likely related to more favorable thermodynamic conditions, which, combined with baroclinic activity, enhance the increase in rainfall intensity. (Escobar et al., 2016).

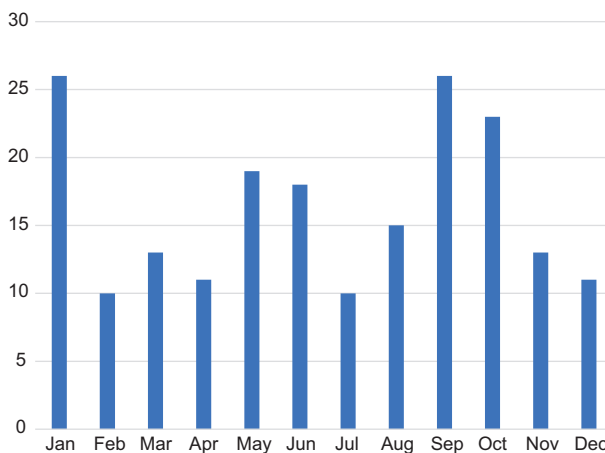


Fig. 2. Annual distribution of the number of cases of HRE in the IVr.

On the other hand, the maximum observed in January (26 cases) could be attributed to the position of the South Atlantic Subtropical Anticyclone (SASA),

which generates northeasterly winds over the study area during this month (Escobar, 2019), leading to HRE in the IVr. Conversely, during February the synoptic pattern associated with the SASA occurs less frequently compared to January (Escobar, 2019), which could explain the observed minimum (10 cases) during this month. The maximum observed in January and the minimum in February were also identified by Escobar et al. (2016) during their study of cold fronts associated with extreme rainfall over the eastern SC state.

3.2 Synoptic climatology associated with HRE in the IVr

3.2.1 Composites fields of atmospheric variables

To identify the primary synoptic features associated with HRE in the IVr, we calculated composites fields for the variables specified in section 2.1. The analysis is based on a sample of 195 HREs, which represents the total number of cases identified during the studied period from 2000 to 2022.

Figure 3 shows the mean synoptic situation associated with HRE in the IVr for days -2 and 0 . The mean sea level pressure shows a cold front located between the SAO and southern Rio Grande do Sul (RS) state on day -2 (Fig. 3a). The frontal system is extended to northeastern Argentina and connected with a large low-pressure system of 1011 hPa, which is located over northern Argentina, Paraguay, and southern Bolivia. This low-pressure system is related to the coupled of the North-Western Argentinean Low (NAL) and the Chaco Low (CHL) (Escobar and Seluchi, 2012). On day 0 (Fig. 3b), the cold front extends from the SAO to eastern Bolivia. The cold front is associated with the extratropical cyclone positioned over the SAO, close to 32° S, 40° W with a center of 1011 hPa. Seluchi et al. (2017) identified a similar surface synoptic pattern when studying the characteristics of cold fronts associated with heavy rainfall in eastern SC.

The frontal characteristics can be confirmed by the thickness gradient observed between the northeast of SC and 32° S, which is consistent with the presence of a frontal system. A similar pattern was found by Teixeira and Satyamurty (2007) and Escobar et al. (2016) when they studied the dynamical and synoptic characteristics of HRE in Southern Brazil and the cold fronts associated with extreme rainfall over the east of SC state, respectively.

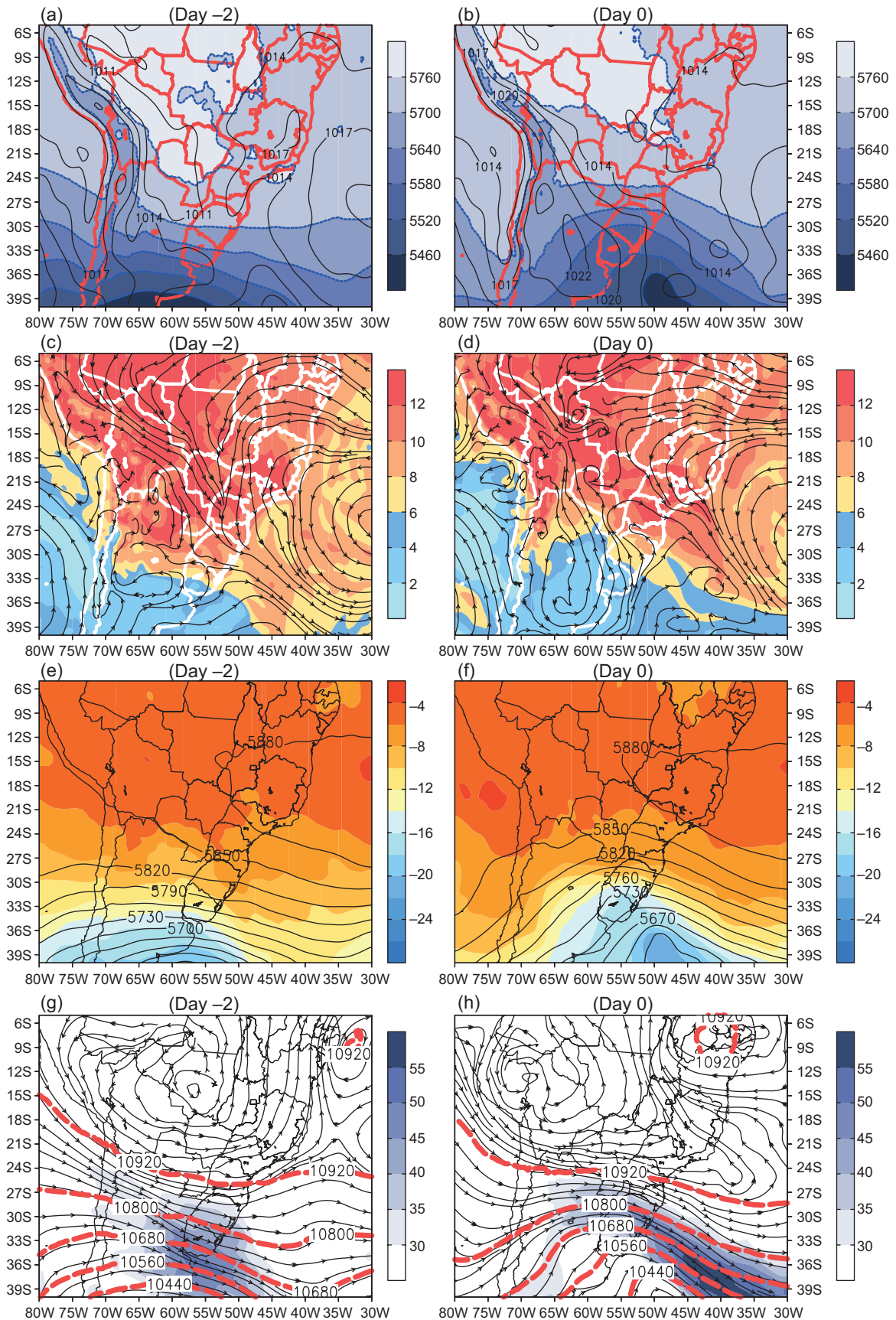


Fig. 3. (a, b) Composite fields of 500/1000 hPa thickness (gpm, shaded) and mean sea level pressure (hPa, black contours); (c, d) streamlines and specific humidity (g kg^{-1} , shaded) at 850 hPa; (e, f) temperature ($^{\circ}\text{C}$, shaded) and geopotential height (gpm) at 500 hPa; (g, h) streamlines, geopotential height (gpm, dashed contours), and isotachs (m s^{-1} , shaded) at 250 hPa. (H: high; L: low). The cold front is represented in blue.

The 850 hPa streamline field shows the position of the cold front in the southern part of RS with northerly and northwesterly winds, transporting warm and moist air from the Amazon basin and the SAO to the state of SC, including the IVr (Fig. 3c). There is also a cyclonic circulation between northern Argentina and southern Bolivia, which is related to the low-pressure area identified at the surface and described in Fig. 3a. Additionally, the cold front is clearly detected through the specific humidity gradient observed in the extreme south and west of Brazil and along the border with Argentina and Uruguay (Fig. 3c).

On day 0 (Fig. 3d), after the passage of the cold front, a decrease in specific humidity is observed over southern and southeastern SC state, with specific humidity values in the range of 8–10 g kg⁻¹. The 500 hPa level shows, on day -2 (Fig. 3e), the frontal trough with its axis extending northwestward from the SAO (40° S, 55° W) to northeastern Argentina (32° S, 60° W). The temperature field shows an intense thermal gradient south of 32° S of approximately 8 °C over a distance of 10° latitude, consistent with the presence of the cold front at middle levels.

On day 0 (Fig. 3f), this frontal trough appears more pronounced, with its axis extending northwestward from the SAO (40° S, 49° W) to the center of Paraguay (25° S, 57° W). The intense thermal gradient moves slightly to the north and is located to the south of 28° S according to the advance of the cold front at low levels (Fig. 3b, d).

It is also possible to observe the phase shift of the thermal wave relative to the mass wave, associated with a typical baroclinic system. This feature is observed mainly on day 0 (Fig. 3f), when the cold front is well-defined.

In the upper troposphere, there is a well-defined frontal trough that accompanies the progress of the cold front at low levels. Two days prior to the HRE (day -2, Fig. 3g), the jet stream exhibits a northwest-southeast orientation around southern Uruguay and northeastern Buenos Aires Province (Argentina), with wind intensities exceeding 45 m s⁻¹. The wide area of strong winds and geopotential height values indicates the coupling of the subtropical jet with the polar jet. Typically, the subtropical jet appears above 10 440 gpm, while the polar jet (north branch) is identified between 10 200 and 10 440 gpm (Escobar et al., 2019a). The polar jet, which is linked to the cold

front at the surface, is observed in close proximity to southern Buenos Aires Province (Argentina) (38° S, 60° W) two days before the HRE (day -2, Fig. 3g).

On the day of the HRE (day 0, Fig. 3h), the frontal trough with its associated jet stream affects a significant portion of RS state, northeastern Argentina, and the SAO, where it shows an intensity of approximately 55 m s⁻¹. This feature is in accordance with an intense horizontal geopotential height gradient. On this day, the presence of the frontal trough is expected to increase upper-level divergence over eastern SC, including the IVr region. This dynamic factor contributes to the intensification of convergence in the lower troposphere, leading to the forced vertical ascent of air from the surface. This mechanism contributes to the intensification of precipitation in the study region.

Another noteworthy feature observed at 250 hPa is an atmospheric circulation pattern similar to the typical upper-level pattern observed during the rainy season in Brazil, characterized by the presence of the Bolivian High and the trough in the northeast region of Brazil. This pattern is common during the rainy season due to its association with strong convective activity in the Amazon basin (Lenters and Cook, 1999). Therefore, it can be inferred that many cases of heavy rainfall occur during the rainy season, as observed in the annual distribution of the number of HRE cases in IVr (Fig. 2).

Figure 4 shows the average infrared field of the GOES family satellite for two days before (day -2) and on the day of the HRE (day 0). Two days earlier (Fig. 4a), a formation of deep clouds was already observed, with a brightness temperature of 264 K, on the south coast of SC. On day 0 (Fig. 4b) the system gained strength, reaching a brightness temperature below 250 K. This temperature indicates the presence of deep clouds associated with a convective system over the ocean. On the other hand, over the study region (Fig. 1a), the temperature was around 252 K. As the average image resolution is 10 km, deep and smaller systems are not discretized. The cloudiness band is extended over the ocean, following the surface frontal band (Fig. 3b) and the specific humidity pattern (Fig. 3d).

Fig. 4c shows the average SST field only on the day of the event (two days before SST anomaly is similar, not shown). Despite what could be expected

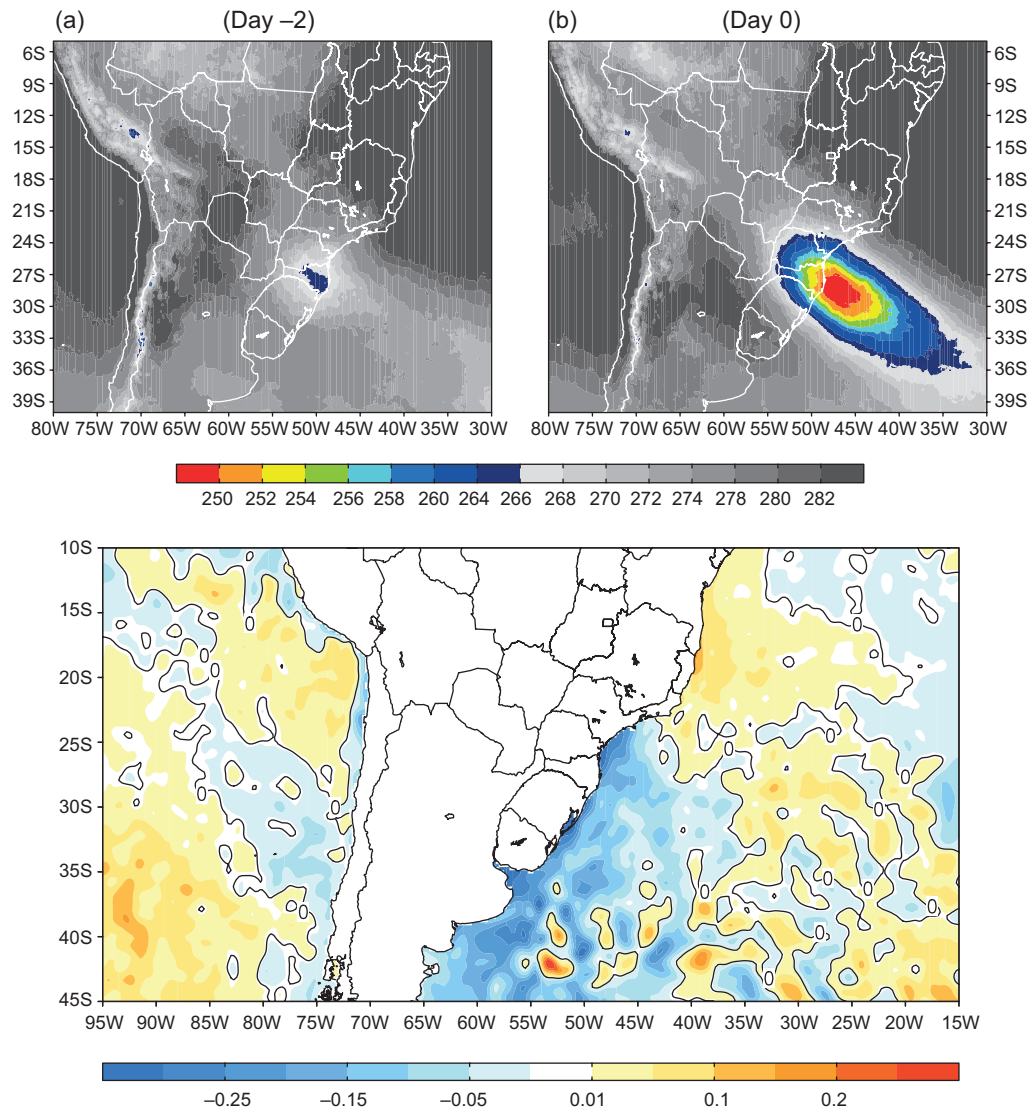


Fig. 4. (a, b) Mean GOES East thermal infrared image (K) HRE composites; (c) sea surface temperature anomalies ($^{\circ}\text{C}$) HRE composites.

in heavy rainfall events on the coast, the SST had a negative anomaly pattern, implying that the ocean was not the main energy that sustained the severe events.

However, the pronounced positive anomalies spread over the South Atlantic around 30°S , 30°W and the observed gradient around 35°S implied that frontal systems would tend to anchor over the area of negative SST anomaly ahead of the coast of southern Brazil and west and south of an area of predominance of positive SST anomalies. It is precisely in the signal

change region (33°S , 40°W) that a closed minimum of pressure was observed (Fig. 3b).

3.2.2 Synoptic patterns associated with HRE in the IVr

The synoptic classification at the surface associated with HRE in the IVr, identified eight PPSs that explain 81.8% of the total variance, with the first four PPSs representing 63.5% of that total (Table I). The remaining PPSs were not considered in the analysis because their series of component loadings presented

Table I. Percentages of explained variance and cumulative percentages explained by the different principal pattern sequences (PPSs).

PPSs	Percentages of explained variance (%)	Cumulative percentages of explained variance (%)
1	18.9	18.9
2	17.8	36.7
3	14.1	50.8
4	12.7	63.5
5	6.4	69.9
6	4.3	74.2
7	3.9	78.1
8	3.7	81.8

values lower than 0.5. The four PPSs associated with HRE in the IVr are shown in Figure 5.

PPS1 (Fig. 5a) explains 18.9% of the total variance. It shows on day -2 a large high-pressure system related to the SASA, which its center positioned at approximately 39° S, 40° W, to the south and west of its average climatological position (Marengo et al., 2012). At the same time, there is a low-pressure area on the continent, extending from the south of Bolivia towards the north and west of Argentina that is related to the coupled of the NAL and the CHL (Escobar and Seluchi, 2012).

During the following days (days -1 and 0), the low-pressure area moves slowly toward the east while intensifying and covering a great part of south-central Brazil. Throughout the entire period, the eastern SC is affected by a horizontal pressure gradient, resulting in northeasterly winds which contribute to intensifying the low-level moisture flux convergence in the region, ultimately leading to heavy rainfall in the IVr.

A similar sequence of surface synoptic patterns was found by Escobar and Reboita (2022) when they studied the main synoptic patterns related to South Atlantic Convergence Zone (SACZ) episodes. The authors found that a day after the occurrence of heavy rainfall in the IVr, the low-pressure area that affects the continent moves toward the SAO while intensifying and producing a cyclone. This low-pressure system contributes to determining a SACZ episode.

PPS2 (Fig. 5b), with 17.8% of the total variance, is associated with the typical passage of a cold front in Brazil (Foss et al., 2017; Escobar, 2019). Two

days before (day -2) of the occurrence of HRE in the IVr, there is a low-pressure system located between northern Argentina, southern Bolivia, and western Paraguay which is probably associated with the CHL. This low-pressure system is connected with a cold front which is extended approximately between the SAO and Uruguay. On this day, a great part of SC state is affected by a westerly and northwesterly wind.

During the following days (day -1 and day 0), the cold front moves northeastward producing southwesterly and southeasterly wind over eastern SC on day -1 and day 0 , respectively. It also can be observed the advance of the post-frontal anticyclone, entering the continent with a meridional component. On day 0 , the cold front is extended between northeastern SC and southwestern Mato Grosso (MT), with the southeasterly wind over the IVr which favors the intensification of the rain over the study area (Fig. 5b).

This sequence of surface synoptic charts is similar to the average of mean sea level pressure associated with HRE in the IVr, obtained through the composite method (Fig. 3b). This result was expected because the PPSs that explain the higher percentage of the total variance are related to the most frequent synoptic pattern, which frequently coincides with the average field (Compagnucci et al., 2001).

PPS3 (Fig. 5c) explains 14.1% of the total variance and also exhibits meteorological features associated with a frontal system, which is linked to a process of cyclogenesis. Two days before the occurrence of HRE in the IVr (day -2), a stationary front appears near eastern SP, extending towards the south and east of Bolivia. Additionally, an elongated region of low pressure, known as an inverted trough, is visible between southern MT and western PR. This surface-level low-pressure system is associated with the formation of a frontal wave.

On the day before the event (day -1), the inverted trough strengthens, and the post-frontal anticyclone moves slightly towards the east, positioning itself near 37° S, 50° W. As a result of this surface atmospheric circulation, the eastern SC region is dominated by easterly winds, which can be quite strong due to an increase in the pressure gradient.

On the day of the event (day 0), the inverted trough continues its eastward movement and can now be found between northeastern MT and northern SP. Additionally, a weak cyclone is observed over

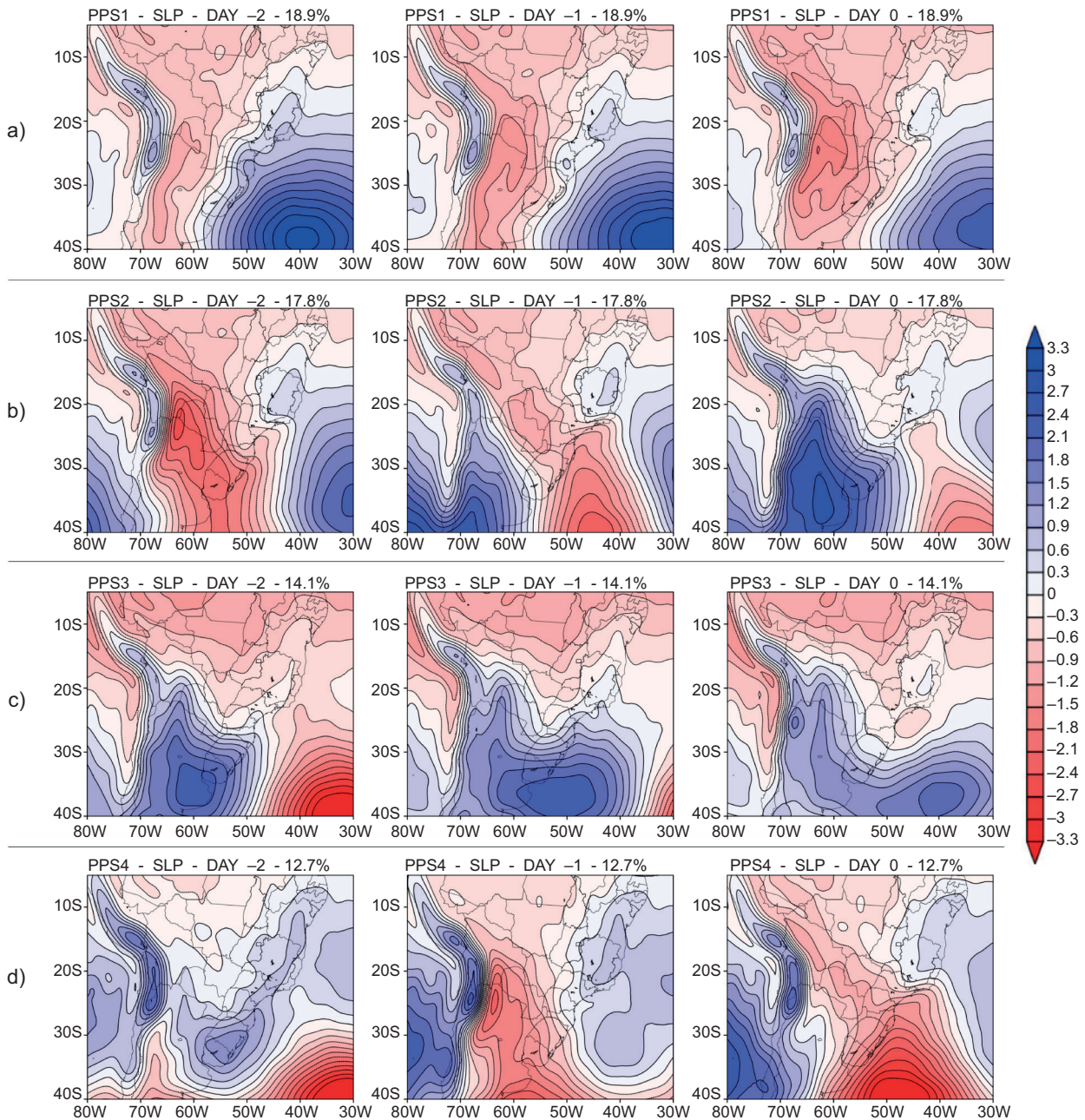


Fig. 5. Principal pattern sequences (PPSs) obtained at surface level. (a) PPS1, (b) PPS2, (c) PPS3, (d) PPS4. From left to right: day -2 , day -1 , and day 0 .

the Atlantic Ocean, located near 25° S, 45° W. This cyclone may develop into an extratropical or subtropical cyclone in the near future. The presence of the cyclone close to the coast of the SC state contributes to increasing the mass and moisture convergence over this area and consequently intensifies the rain in the IVr.

A similar synoptic weather pattern was identified by Escobar et al. (2019b) and Escobar (2023) when they conducted a synoptic climatology of winter over Brazil and a synoptic classification associated with “friagens” in central-western Brazil, respectively.

The last main surface synoptic pattern, as shown in PPS4 (Fig. 5d), accounts for 12.7% of the total

variance and is associated with a meteorological situation characterized by the presence of a cold front across the study area. Unlike PPS2 in Figure 5b, which is also related to a cold front, the main difference lies in the location of the frontal system. In PPS2, the frontal system is positioned around the eastern SP on day 0, generating southeasterly winds in IVr. In contrast, the cold front in PPS4 is in the east of SC state, creating southwesterly winds in IVr.

Therefore, the passage of a cold front can lead HRE in the IVr with southwesterly or southeasterly winds. When the cold front is accompanied by southeasterly winds (PPS2, Fig. 5b), there is greater interaction between the low-level flow and the complex topography of the region, resulting in more intense rainfall in the study area. Furthermore, this surface synoptic pattern (PPS2, Fig. 5b) occurs more frequently than the other pattern (PPS4, Fig. 5d) because it explains a higher percentage of the variance (Table I). These two synoptic patterns associated with the presence of a cold front were also found by Escobar et al. (2016) when they performed a synoptic climatology of cold fronts associated with HRE in the IVr.

The distribution of variance explained by the first four sequence patterns across different seasons is presented in Table II.

Table II. Percentages of total explained variance and variance accumulated by the first four principal pattern sequences (PPSs) during the different seasons of the year, associated with heavy rainfall events in the Itajaí Valley region.

Season	PPS1	PPS2	PPS3	PPS4
Summer	5.5	4.2	1.5	2.6
Autum	4.8	3.7	4.2	1.9
Winter	1.7	4.0	3.9	3.7
Spring	6.9	5.8	4.3	4.4
Total	18.9	17.8	14.1	12.7

Summer (December, January, February), autumn (March, April, May), winter (June, July, August), spring (September, October, November).

Spring exhibits the highest percentages of explained variance, with PPS1 and PPS2 having the greatest values (6.9 and 5.8, respectively). PPS1

shows a significant contribution throughout the year, except for winter, which has a lower value (1.7) of explained variance. This result is consistent because from October to March, the SASA tends to be located further south, promoting the occurrence of blocking situations (Escobar, 2019; Escobar and Reboita, 2022). Consequently, this surface synoptic pattern leads to persistent easterly/northeasterly winds affecting the eastern SC, resulting in an increase in HRE in the IVr.

PPS3 is the only sequence pattern that hardly appears during summer, representing the lowest percentages of explained variance (1.5). This pattern is typically associated with cold surges in South America between May and September.

Figure 6 shows examples of the synoptic surface charts (prepared by the weather forecasters from the CPTEC/INPE) highly correlated with the four PPSs associated with HRE in the IVr. The synoptic surface chart associated with the patterns PPS1 (D0) (Fig. 6a) shows the SASA centered around 43° W, 38° S, with an inverted trough embedded in it that sits over the northern RS. This surface circulation pattern resembles a blocking configuration with northeasterly winds over the eastern SC, which promotes the intensification of heavy rain in the IVr.

The synoptic charts associated with the remaining patterns indicate a cold front, leading to mass and moisture convergence towards the eastern SC. In particular, the synoptic surface chart linked to the PPS2 (day 0) pattern (Fig. 6b) displays south-southeasterly winds over the study area, while the chart related to PPS4 (day 0) (Fig. 6d) shows southwesterly winds. Conversely, the synoptic chart connected to PPS3 (day 0) (Fig. 6c) shows an extratropical frontal wave, with the cyclone positioned near the coast of the SC state, resulting in easterly winds in the study region.

4. Conclusions

This study investigated the synoptic characteristics associated with the occurrence of HRE in the IVr, over the eastern part of SC state. Over the entire period analyzed, a total of 195 HRE were identified in the IVr, corresponding to accumulations greater than 27 mm per day.

The season with the greatest occurrence of HRE in the IVr region was spring, which can be attributed to more favorable thermodynamic conditions that,

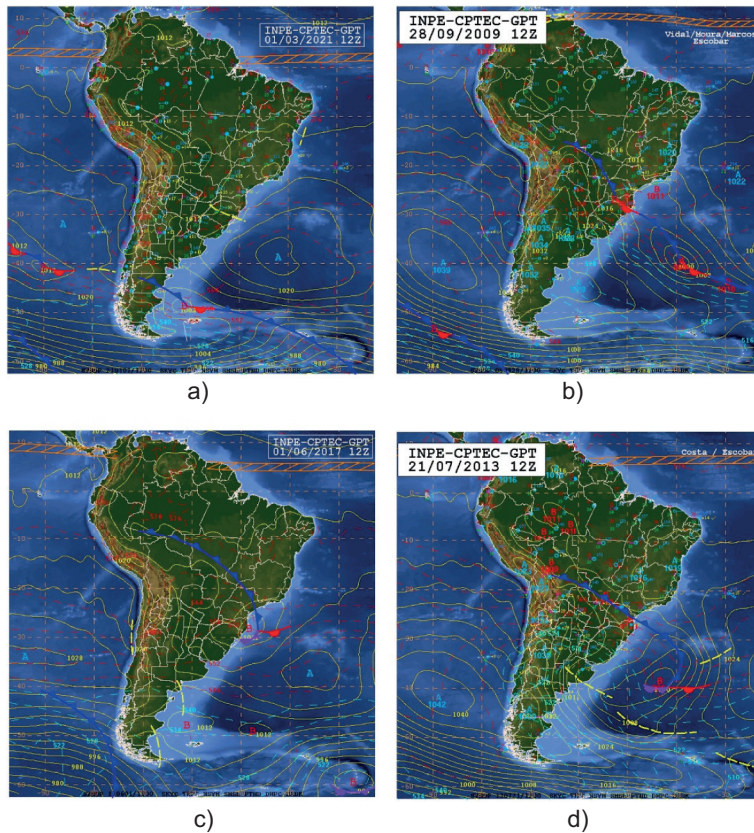


Fig. 6. Surface synoptic charts elaborated by the Brazilian Center for Weather Forecast and Climate Studies (CPTEC)/National Institute for Space Research (INPE) at 12:00 UTC associated with HRE in the IVr (day 0). (a) March 01, 2021; (b) September 28, 2009; (c) June 01, 2017; (d) July 21, 2013. Sea level pressure (hPa) in continuous yellow lines and 1000-500 hPa thickness in red dashed lines. Synoptic symbols as in conventional mode.

when combined with baroclinic activity, enhance the intensity of rainfall.

The mean synoptic pattern associated with HRE in the IVr was characterized by the advance of a typical cold front, which was observed over southern RS on day -2 and around the northeast of SC on day 0. On day -2 , the NAL and CHL were present, both of which promoted warm advection over the western part of SC state. This finding aligns closely with the results reported by Seluchi et al. (2017) in their study about the characteristics of cold fronts linked to heavy rainfall in eastern SC.

On day -2 , the atmospheric circulation at 850 hPa showed northerly and northwesterly winds transporting warm and moist air from the Amazon basin and the SAO to the state of SC, including the IVr. The NAL and CHL were also identified at this level through the presence of a cyclonic circulation between northern Argentina and southern Bolivia.

The atmospheric circulation in the middle and upper troposphere (500 and 250 hPa) revealed a

well-defined frontal trough accompanying the progress of the cold front at low levels. During the analyzed period (from day -2 to day 0), it can be observed the advance of a typical baroclinic system with the phase shift of the thermal wave relative to the mass wave.

The mean atmospheric circulation at 250 hPa showed a configuration pattern similar to the typical upper-level pattern observed during the rainy season in Brazil, which means that many cases of heavy rainfall occur during this period of the year.

On day 0, the IVr is influenced by the upper-level atmospheric circulation, which leads to a divergence aloft. This phenomenon results in the intensification of rainfall in the study region.

The analysis of the mean GOES East thermal infrared field identified during the analyzed period a cloudiness band related to the mean position of the frontal system. On day 0 in the IVr, the deep clouds revealed an intense convective system, reaching a brightness temperature below 250 K over the eastern SC and adjacent Atlantic Ocean.

The SST, on the other hand, showed a negative anomalous pattern, indicating that it is not the configuration that provides the necessary energy for the event's intensity, but rather the pattern of continental circulation with moisture transport from the interior of the continent. However, the positive anomaly pattern further north and west may have acted as an anchor for the frontal systems.

The surface synoptic classification associated with HRE in the IVr revealed four main synoptic patterns, which accounted for 63.5% of the total variance. Two of these patterns (PPS2 and PPS4) corresponded to the displacement of a cold front that reaches the eastern SC on day 0, accounting for 17.8 and 12.7% of the total variance, respectively. The surface synoptic charts associated with PPS2 were similar to the average mean sea level pressure associated with HRE in the IVr, obtained through the composite method. On day 0, the cold front was positioned around the eastern SP, leading to southeasterly winds in the IVr. In contrast, the cold front in PPS4 was located in the east of SC state, resulting in southwesterly winds in the IVr. These results indicated that HRE in the IVr occurs during and after the cold front passes over the SC state. These two synoptic patterns, correlated with the presence of a cold front, were also identified by Escobar et al. (2016) during their synoptic climatology analysis of cold fronts associated with HRE in the IVr.

PPS1 accounted for 18.9% of the total variance and was related to the SASA, which was situated south of its climatological position during the analyzed period. With this surface circulation, northeasterly winds affected the eastern SC, intensifying the low-level moisture flux convergence over this area and resulting in HRE in the IVr. This synoptic pattern, associated with an atmospheric blocking configuration, significantly contributed during the rainy season (October to March), and it was also identified by Escobar et al. (2022) in their study of the main synoptic patterns related to SACZ episodes.

The last main synoptic pattern was the PPS3, which explained 14.1% of the total variance and was linked to a process of cyclogenesis. On the day of the HRE (day 0), the cyclonic circulation of the low-pressure system located to the east of SC state contributed to increasing the mass and moisture convergence

over this area and consequently intensified the rain in the IVr. This synoptic pattern is typically associated with cold surges in South America between May and September. It is similar to those identified by Escobar and Reboita (2022) in their study about the synoptic climatology of winter over Brazil and by Escobar et al. (2019) in their synoptic classification associated with friagens in central-west Brazil.

It is important to highlight that this paper introduces novelties related to HRE in the IVr compared to other authors. In this manuscript, in addition to confirming findings from previous studies, we were also able to identify the principal modes of daily variation in atmospheric circulation associated with HRE in the IVr.

Finally, it is noteworthy that the results obtained in this study are useful for weather forecasters working in operational weather centers that have to predict the heavy rainfall occurring in the IVr.

Acknowledgments

The authors thank the National Institute for Space Research (INPE) of Brazil for the synoptic charts and satellite images. We also express our gratitude to the National Center for Environmental Prediction (NCEP) for the reanalysis data and the Brazilian Research Council (CNPq) for financial support (Edital Universal grant number 402554/2021-3).

References

- Andrade KM. 2005. Climatologia e comportamento dos sistemas frontais sobre a América do Sul. M.Sc. thesis. Instituto Nacional de Pesquisas Espaciais (INPE), Brazil.
- Ávila MRR, Mattedi MA. 2017. Disaster and territory: The production of vulnerability to disasters in the city of Blumenau/SC. *Revista Brasileira de Gestão Urbana* 9: 18-202. <https://doi.org/10.1590/2175-3369.009.002.AO03>
- Cardoso de Souza C. 2017. Abrangência e persistência de eventos extremos de precipitação no sul do Brasil: El Niño Oscilação Sul e padrões atmosféricos. Ph.D. thesis. Universidade Federal de Santa Catarina, Brazil.
- Cattell RB. 1978. The scientific use of factor analysis in behavioral and life sciences. Plenum Press, New York and London. <https://doi.org/10.1007/978-1-4684-2262-7>

- Compagnucci RH, Salles MA. 1997. Surface pressure patterns during the year over southern South America. *International Journal of Climatology* 17: 635-653. [https://doi.org/10.1002/\(SICI\)1097-0088\(199705\)17:6<635::AID-JOC81>3.0.CO;2-B](https://doi.org/10.1002/(SICI)1097-0088(199705)17:6<635::AID-JOC81>3.0.CO;2-B)
- Compagnucci RH, Araneo D, Canziani PO. 2001. Principal sequence pattern analysis: A new approach to classifying the evolution of atmospheric systems. *International Journal of Climatology* 21: 197-217. <https://doi.org/10.1002/joc.601>
- Da Silva Dias MAF. 2009. As chuvas de novembro de 2008 em Santa Catarina: um estudo de caso visando à melhoria do monitoramento e da previsão de eventos extremos. INPE, São José dos Campos, Brazil. Available at: <http://urlib.net/sid.inpe.br/mtc-m19@80/2009/11.05.11.33>
- Dereczynski CP, de Oliveira JS, Machado CO. 2009. Climatologia da precipitação no município do Rio de Janeiro. *Revista Brasileira de Meteorologia* 24: 24-38. <https://doi.org/10.1590/S0102-77862009000100003>
- Escobar G, Compagnucci R, Bischoff S. 2004. Sequence patterns of 1000 hPa and 500 hPa geopotential height fields associated with cold surges in Buenos Aires. *Atmósfera* 17: 69-89.
- Escobar GCJ, Seluchi ME. 2012. Classificação sinótica dos campos de pressão atmosférica na América do Sul e sua relação com as Baixas do Chaco e do Noroeste Argentino. *Revista Brasileira de Meteorologia* 27: 365-375. <https://doi.org/10.1590/S0102-77862012000300011>
- Escobar GCJ, Seluchi ME, Andrade K. 2016. Classificação sinótica de frentes frias associadas a chuvas extremas no leste de Santa Catarina (SC). *Revista Brasileira de Meteorologia* 31: 649-661. <https://doi.org/10.1590/0102-7786312314b20150156>
- Escobar GCJ. 2019. Classificação sinótica durante a estação chuvosa do Brasil. *Revista Anuário do Instituto de Geociências (UFRJ)* 42: 421-436. http://doi.org/10.11137/2019_2_421_436
- Escobar GCJ, Reboita MS, Souza A. 2019a. Climatology of surface baroclinic zones in the coast of Brazil. *Atmósfera* 32: 129-141. <https://doi.org/10.20937/ATM.2019.32.02.04>
- Escobar GCJ, Vaz JCM, Reboita MS. 2019b. Surface atmospheric circulation associated with “Frigens” in Central-West Brazil. *Anuário do Instituto de Geociências (UFRJ)* 42: 241-254. https://doi.org/10.11137/2019_1_241_254
- Escobar GCJ, Reboita MS. 2022. Relationship between daily atmospheric circulation patterns and South Atlantic Convergence Zone (SACZ) events. *Atmósfera* 35: 1-25. <https://doi.org/10.20937/ATM.52936>
- Escobar GCJ, de Almeida Marques AC, Dereczynski CP. 2022. Synoptic patterns of South Atlantic Convergence Zone episodes associated with heavy rainfall events in the city of Rio de Janeiro, Brazil. *Atmósfera* 35: 287-305. <https://doi.org/10.20937/ATM.52942>
- Escobar GCJ. 2023. Classification of wintertime daily atmospheric circulation patterns over Brazil. *Atmósfera* 37: 345-363. <https://doi.org/10.20937/ATM.53176>
- Fortunato de Faria L, Reboita MS, Mattos EV, Carvalho VSB, Martins Ribeiro JG, Capucin BC, Drumond A, Paes dos Santos AP. 2023. Synoptic and mesoscale analysis of a severe weather event in southern Brazil at the end of June 2020. *Atmosphere* 14: 486. <https://doi.org/10.3390/atmos14030486>
- Foss M, Chou SC, Seluchi ME. 2017. Interaction of cold fronts with the Brazilian plateau: A climatological analysis. *International Journal of Climatology* 37: 3644-3659. <https://doi.org/10.1002/joc.4945>
- García CM, Roseghini WFF, Aschidamini IM. 2011. Environmental management planning – Considerations about the events occurring in Santa Catarina – Brazil in November 2008. *Procedia Social and Behavioral Sciences* 19: 487-493. <https://doi.org/10.1016/j.sbspro.2011.05.159>
- Gozzo LF, da Rocha RP, Reboita MS, Sugahara S. 2014. Subtropical cyclones over the southwestern South Atlantic: Climatological aspects and case study. *Journal of Climate* 27: 8543-8562. <https://doi.org/10.1175/JCLI-D-14-00149.1>
- Green PE, Carroll JD. 1978. *Analyzing multivariate data*. The Dryden Press, Illinois.
- Harman HH. 1976. *Modern factor analysis*. The University of Chicago Press, Chicago, IL.
- Herrmann MLP. 2014. *Atlas de desastres naturais do Estado de Santa Catarina: Período de 1980 a 2010*. 2nd ed. Cadernos Geográficos (GCN/UFSC). Instituto Histórico e Geográfico de Santa Catarina Florianópolis (IHGSC), Florianópolis, Brazil. .
- Hoskins BJ, Hodges KI. 2005. A new perspective on the Southern Hemisphere storm tracks. *Journal of Climate* 18: 4108-4129. <https://doi.org/10.1175/JCLI3570.1>
- Huang B, Liu C, Banzon V, Freeman E, Graham G, Hankins B, Smith T, Zhang H. 2021. Improvements of the daily optimum interpolation sea surface tem-

- perature (DOISST) version 2.1. *Journal of Climate* 34: 2923-2939. <https://doi.org/10.1175/JCLI-D-20-0166.1>
- Huth R, Beck C, Philipp A, Demuzere M, Ustrnul Z, Cahynová M, Kyselý J, Tveito OE. 2008. Classifications of atmospheric circulation patterns: Recent advances and applications. *Trends and Directions in Climate Research: Annals of the New York Academy of Sciences* 1146: 105-152. <https://doi.org/10.1196/annals.1446.019>
- Knapp KR, Ansari S, Bain CL, Bourassa MA, Dickinson MJ, Funk C, Helms CN, Hennon CC, Holmes CD, Huffman GJ, Kossin JP, Lee H-T, Loew A, Magnusdottir G. 2011. Globally gridded satellite observations for climate studies. *Bulletin of the American Meteorological Society* 92: 893-907. <https://doi.org/10.1175/2011BAMS3039.1>
- Lenters JD, Cook KH. 1999. Summertime precipitation variability over South America: Role of the large-scale circulation. *Monthly Weather Review* 127: 409-431. [https://doi.org/10.1175/1520-0493\(1999\)127%3C0409:SPVOSA%3E2.0.CO;2](https://doi.org/10.1175/1520-0493(1999)127%3C0409:SPVOSA%3E2.0.CO;2)
- Lim EP, Simmonds I. 2002. Explosive cyclone development in the Southern Hemisphere and a comparison with Northern Hemisphere events. *Monthly Weather Review* 130: 2188-2209. [https://doi.org/10.1175/1520-0493\(2002\)130<2188:EC-DITS>2.0.CO;2](https://doi.org/10.1175/1520-0493(2002)130<2188:EC-DITS>2.0.CO;2)
- Marengo JA, Liebmann B, Grimm AM, Misra V, Silva Dias PL, Calvalcanti IFA, Carvalho LMV, Berbery EH, Ambrizzi T, Vera CS, Saulo AC, Noguez-Paegle J, Zipser E, Seth A, Alves LM. 2012. Recent developments on the South American monsoon system. *Review. International Journal of Climatology* 32: 1-21. <https://doi.org/10.1002/joc.2254>
- McTaggart-Cowan R, Bosart LF, Davis CA, Atallah EH, Gyakum JR, Emanuel KA, 2006. Analysis of hurricane Catarina (2004). *Monthly Weather Review* 134: 3029-3053. <https://doi.org/10.1175/MWR3330.1>
- Murara P, Acquavotta F, Garzena D, Fratianni S. 2018. Daily precipitation extremes and their variations in the Itajaí River Basin, Brazil. *Meteorology and Atmospheric Physics* 131: 1145-1156. <https://doi.org/10.1007/s00703-018-0627-0>
- Reboita MS, Gozzo LF, Crespo NM, Custodio MS, Lucyrio V, de Jesus EM, da Rocha RP. 2022. From a Shapiro-Keyser extratropical cyclone to the subtropical cyclone Raoni: An unusual winter synoptic situation over the South Atlantic Ocean. *Quarterly Journal of the Royal Meteorological Society* 148: 2991-3009. <https://doi.org/10.1002/qj.4349>
- Richman M. 1986. Rotation of principal components. *Journal of Climatology* 6: 293-335. <https://doi.org/10.1002/joc.3370060305>
- Richman M, Angel J, Gong X. 1992. Determination of dimensionality in eigenanalysis. In: *Proceedings of the 5th International meeting on statistical climatology*, Toronto, Canada.
- Rozante JR, Moreira DS, de Gonçalves LGG, Vila DA. 2010. Combining TRMM and surface observations of precipitation: Technique and validation over South America. *Weather and Forecasting* 25: 885-894. <https://doi.org/10.1175/2010WAF2222325.1>
- Saha S, Moorthi S, Pan H, Wu X, Wang J, Nadiga S, Tripp P, Kistler R, Woollen J, Behringer D, Liu H, Stokes D, Grumbine R, Gayno G, Wang J, Hou Y, Chuang H, Juang HH, Sela J, Iredell M, Treadon R, Kleist D, Van Delst P, Keyser D, Derber J, Ek M, Meng J, Wei H, Yang R, Lord S, van den Dool H, Kumar A, Wang W, Long C, Chelliah M, Xue Y, Huang B, Schemm J, Ebisuzaki W, Lin R, Xie P, Chen M, Zhou S, Higgins W, Zou C, Liu Q, Chen Y, Han Y, Cucurull L, Reynolds RW, Rutledge G, Goldberg M. 2010. The NCEP Climate Forecast System Reanalysis. *Bulletin of the American Meteorological Society* 91: 1015-1057. <https://doi.org/10.1175/2010BAMS3001.1>
- Saha S, Moorthi S, Wu X, Wang J, Nadiga S, Tripp P, Behringer D, Hou Y, Chuang H, Iredell M, Ek M, Meng J, Yang R, Mendez MP, van den Dool H, Zhang Q, Wang W, Chen M, Becker E. 2014. The NCEP Climate Forecast System Version 2. *Journal of Climate* 27: 2185-2208. <https://doi.org/10.1175/JCLI-D-12-00823.1>
- Sanders F, Gyakum JR. 1980. Synoptic-dynamic climatology of the "Bomb". *Monthly Weather Review* 108: 1589-1606. [https://doi.org/10.1175/1520-0493\(1980\)108<1589:SDCOT>2.0.CO;2](https://doi.org/10.1175/1520-0493(1980)108<1589:SDCOT>2.0.CO;2)
- Seluchi ME, Saulo AC. 1998. Possible mechanisms yielding an explosive coastal cyclogenesis over South America: Experiments using a limited area model. *Australian Meteorological Magazine* 47: 309-320.
- Seluchi M, Beu C, Andrade KM. 2017. Características das Frentes Frias Causadoras de Chuvas Intensas no Leste de Santa Catarina. *Revista Brasileira de Meteorologia* 32: 25-37. <https://doi.org/10.1590/0102-778632120150095>
- Silva Dias MAF. 2009. As chuvas de novembro de 2008 em Santa Catarina: Um estudo de caso visando melhoria

- do monitoramento e da previsão de eventos extremos. INPE, São José dos Campos, Brazil. Available at: <http://urlib.net/sid.inpe.br/mtc-m19@80/2009/11.05.11.33>
- Silva ED, Reboita MS. 2013. Estudo da Precipitação no Estado de Minas Gerais – MG. *Revista Brasileira de Climatologia* 13: 120-136. <https://doi.org/10.5380/abclima.v13i0.33345>
- Simmonds I, Keay K. 2000. Mean Southern Hemisphere extratropical cyclone behavior in the 40-year NCEP-NCAR reanalysis. *Journal of Climate* 13: 873-885. [https://doi.org/10.1175/1520-0442\(2000\)013%3C0873:MSHECB%3E2.0.CO;2](https://doi.org/10.1175/1520-0442(2000)013%3C0873:MSHECB%3E2.0.CO;2)
- Taljaard JJ. 1972. Synoptic meteorology of the Southern Hemisphere. In: *Meteorology of the Southern Hemisphere* (Newton CW, Ed.). Meteorological Monographs 13. American Meteorological Society, Boston, MA, 139-213. https://doi.org/10.1007/978-1-935704-33-1_8
- Teixeira MD, Satyamurty P. 2007. Dynamical and Synoptic Characteristics of Heavy Rainfall Episodes in Southern Brazil. *Monthly Weather Review* 135, 598-617. <https://doi.org/10.1175/MWR3302.1>